Hindawi
Wireless Communications and Mobile Computing
Volume 2018, Article ID 8131705, 8 pages
https://doi.org/10.1155/2018/8131705

Research Article

Miniature Multiband Inverted-F Antenna over an Electrically Small Ground Plane for Compact IoT Terminals

Leonardo Lizzi,[1] **Fabien Ferrero**,[1] **Christophe Danchesi**,[2] **and Stephane Boudaud**[2]

[1] *Université Côte d'Azur, CNRS, LEAT, 930 route des Colles, 06903 Sophia Antipolis, France*
[2] *Abeeway, 635 route des Lucioles, 06560 Valbonne, France*

Correspondence should be addressed to Leonardo Lizzi; leonardo.lizzi@unice.fr

Received 29 March 2018; Accepted 14 June 2018; Published 4 July 2018

Academic Editor: Eva Antonino-Daviu

This paper describes the design of a miniaturized multiband Inverted-F Antenna (IFA) suitable for integration in compact Internet-of-things (IoT) terminals. The antenna efficiently operates over the LoRa (915 MHz) and GPS L1 (1.57 GHz) and L2 (1.23 GHz) bands. Its dimensions are $13 \times 25 \times 1$ mm^3 ($0.04\lambda \times 0.08\lambda \times 0.003\lambda$ compared to the lower operating frequency) for a total device size of $40 \times 25 \times 10$ mm^3. Measurements of the antenna when integrated into an IoT position tracking device as well as of the whole terminal in a real application scenario are reported.

1. Introduction

Historically, the term "mobile terminals" has been dedicated to cellular phone applications. In the last decade, with the development of new wireless communication systems and services, this term now covers a wide variety of devices such as tablets, smartwatches, headsets, gamepad controllers, and global positioning system (GPS) receivers. This evolution has been literally exploded with the spreading of the Internet-of-things (IoT) idea, in which any object can be connected to the Internet sharing information over the network.

The design of antennas for mobile terminals has always attracted great attention from the scientific community. In the last years, several works have been aimed at proposing miniaturized radiating systems characterized by good radiation efficiency and multiband operation. One of the most used antenna structures is the Inverted-F Antenna and its variations [1]; however, other solutions based on magnetoelectric monopoles [2], notch antennas [3], coupled apertures [4], or exploiting the shielding box of the mobile terminal [5] have been proposed. Since the compactness of modern mobile terminals limits the dimension of the antenna ground plane, this latter has to be numerically modeled and considered during the design process of the antenna. Starting from this consideration, techniques for reducing the volume of the antenna by efficiently utilizing the radiation of the currents on the terminal chassis [6] or improving the antenna performance by properly modifying the current distribution on the ground plane [7, 8] have been proposed.

The great majority of the works available in literature, however, consider terminal dimensions comparable to those of a commercial smartphone. To the best of authors' knowledge, small research effort has been made in dealing with smaller terminals, such as for IoT applications. This could seem to be a small difference; however, in practice, the efficiency of the antenna can be limited by the use of a small ground plane. This point will be discussed later in the paper with reference to the proposed antenna design. One of the few available examples is represented by the work in [9], where an electrically small loop antenna standing on a compact ground plane and integrated into a wireless sensor package is presented. Because of the very small dimensions of the terminal device compared to the operating wavelength, the packaging of the device has been also considered during the design of the antenna. Despite the acceptable performance of the proposed solution, the choice of a 3D geometry makes the antenna less suitable for mass production of IoT devices, for which printed solutions are preferred.

In the paper, starting from the preliminary results presented in [10], the design of a printed multiband antenna suitable for compact IoT mobile terminals is presented. The integration of the antenna into the final device has

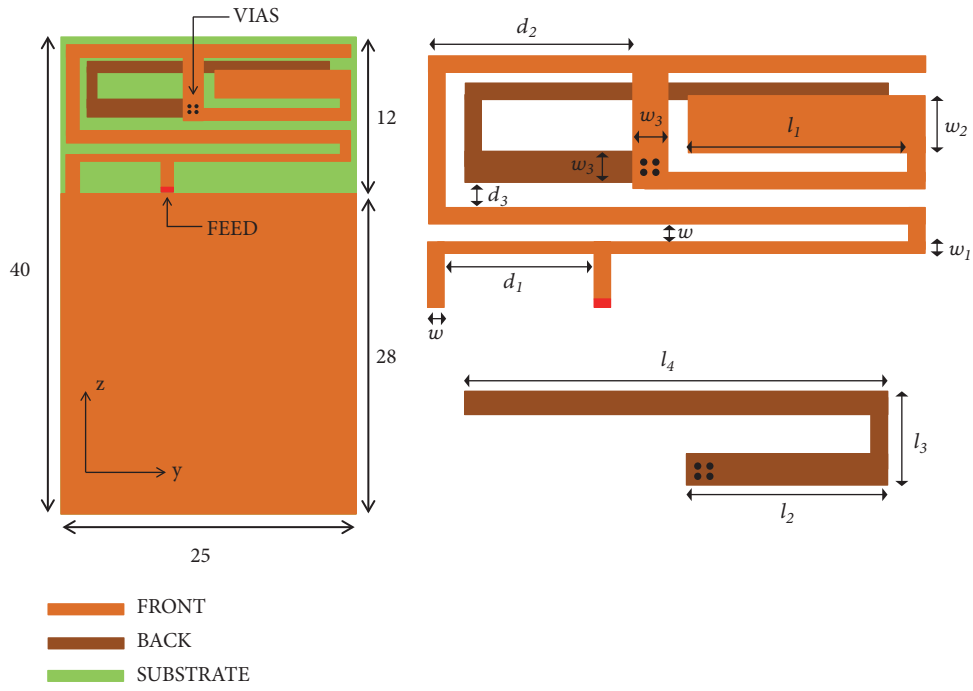

Figure 1: PCB layout (left) and zoom on the antenna geometry (right).

been carefully considered and all the different components constituting the device have been modeled and taken into account in optimizing the antenna. Differently from [10], where only the impedance matching analysis was reported, the present paper completely characterizes the proposed antenna, analyzing the effect of the small ground plane and providing the measured radiation behavior of the proposed antenna when integrated into the final IoT device. Moreover, the performance of the device when employed in a realistic application scenario has been experimentally evaluated.

2. Antenna Design

The considered IoT mobile terminal is a compact position tracking device. Attached to an object (e.g., keys, luggage), this device must be capable of obtaining its localization information through a GPS receiver and sending the data using LoRa communication standard.

In order to guarantee the operation over the GPS and LoRa standards, the antenna is required to exhibit a good impedance matching at $f_{\mathrm{LB}} = 915$ MHz, $f_{\mathrm{MB}} = 1.23$ GHz, and $f_{\mathrm{HB}} = 1.57$ GHz. To keep the device dimensions as compact as possible, the space available for the antenna is limited to 12×25 mm^2, corresponding to $0.04\lambda \times 0.08\lambda$ at f_{LB}. As shown in Figure 1, such space is located at the top of a 40×25 mm^2 (equivalent to $0.12\lambda \times 0.08\lambda$) printed circuit board (PCB). The PCB is made of FR4 dielectric substrate ($\varepsilon_r = 4.3$ and $\tan\delta = 0.025$) of 1 mm thickness. The remaining part of the PCB is dedicated to the electronic circuitry of the device. Its back side is covered with metal and it should act as a ground plane for the antenna. However, because of its very compact dimensions, this metallic part actively contributes to the antenna radiation behavior and it must be rather considered as the second arm of an asymmetrical dipole (the first arm being the actual antenna). The structure of the antenna is shown in Figure 1 on the right. It is based on a meandered Inverted-F Antenna (IFA) in which a slot has been inserted (front layer) to obtain multiple resonances necessary for multiband operation. In order to exploit the limited available space, 4 vias are used to extend the meandered structure on the other side of the substrate (back layer). The use of multiple vias in parallel allows the reduction of the effective contact resistance, thus reducing the antenna losses. The antenna geometrical parameters are indicated in Figure 1. As not differently indicated, all the lines widths and gaps are characterized by the same value w.

This geometry, when excited as shown in Figure 1, generates three different resonant frequencies that can be used to cover the requested bands. The three resonances are visible in Figure 2(a) where the input impedance of the antenna is reported. To better understand the functioning of the antenna, Figure 2(b) shows the surface current distributions at the three resonant frequencies on the antenna metallic parts on the front (left) and back (right) of the substrate. As expected, the resonant frequency used for the lower band (f_{LB}) depends on the IFA total length. Differently, the highest resonance at f_{HB} is controlled by the dimension of the slot on the front side of the antenna, while weak currents flow on the IFA arm on the back side. Finally, the medium band resonance at f_{MB} is a higher order mode of the lower resonance, which is shifted towards the low frequencies because of the coupling with the slot.

Based on this analysis, the antenna geometrical parameters have been optimized to fix the resonances over the

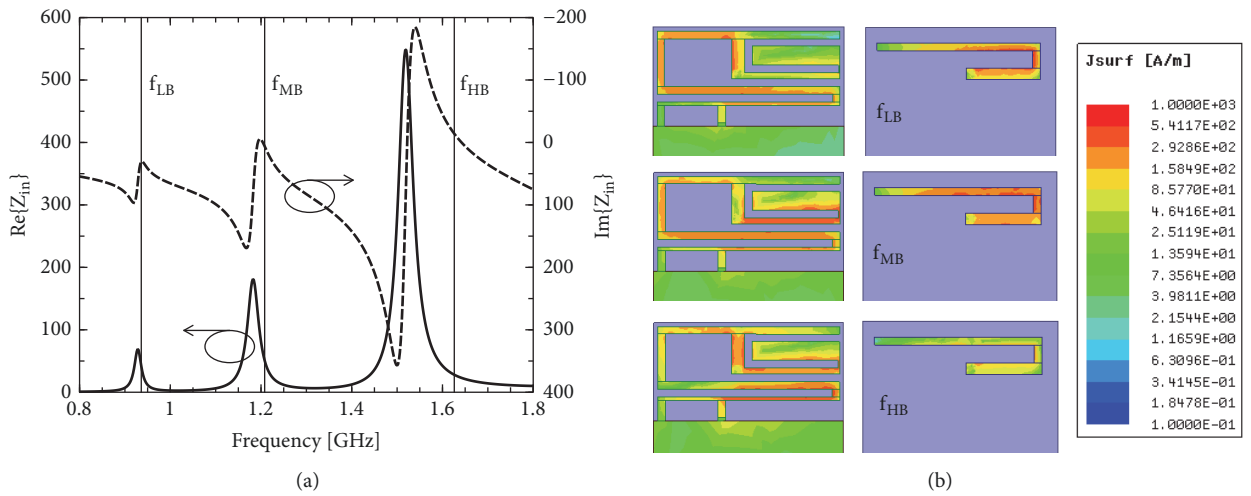

FIGURE 2: (a) Antenna input impedance and (b) surface current distribution at the resonant frequencies.

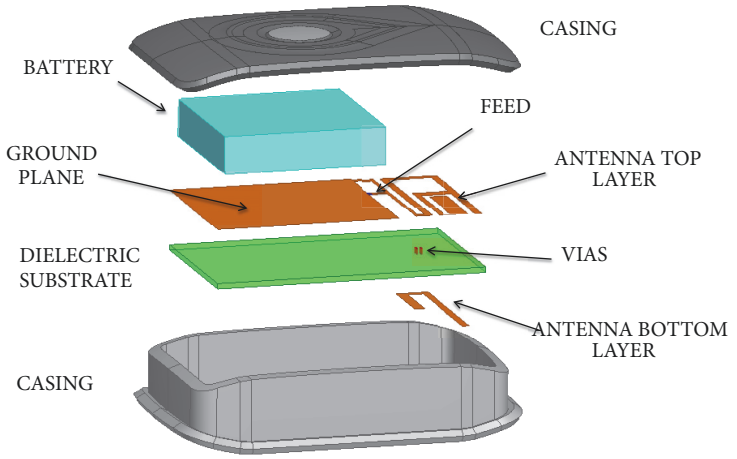

FIGURE 3: Numerical model of the IoT terminal.

requested bands. Since the antenna resonance behavior is controlled by few parameters, a simple trial and error optimization procedure has been used. To take into account the effects given by the environment close to the antenna, a simplified model of the IoT device including the casing and the battery has been realized and considered in the optimization process (Figure 3). The casing has been modeled as a box of lossless plastic material ($\varepsilon_r = 2.6$) surrounding the PCB, while the battery has been modeled as being fully made of copper.

Figure 4 shows the parametric study performed on the two main geometrical parameters (the IFA total length and the slot dimension) highlighted by the surface current analysis reported in Figure 2(b). In Figure 4(a), the total IFA length is varied by modifying the value of the l_4 segment. As can be noticed, as l_4 increases, f_{LB} decreases, while f_{HB} stays unchanged. The optimal l_4 value for which $f_{LB} = 915$ MHz is found for $l_4 = 21.5$ mm. In Figure 4(b), the slot dimension is modified by varying the l_1 value. As expected, when l_1 is increased, f_{HB} shifts to the lower frequencies, while the position of f_{LB} does not change. The optimal l_1 value for which $f_{HB} = 1.57$ GHz is found for $l_1 = 11.5$ mm. Similar parametric studies (not reported here) have been performed for the remaining antenna parameters shown in Figure 1. The final result is an optimized antenna geometry exhibiting three resonant frequencies with good impedance matching ($VSWR \leq 2.5$) at the three requested operating bands. The optimized values of all the antenna geometrical parameters are reported in Table 1.

Figure 5(a) shows the impedance matching of the optimized antenna in terms of voltage standing wave ratio (VSWR). The comparison between the case of the antenna in isolation and when integrated into the device is reported. As can be observed, the integrated antenna is well matched over the LoRa and GPS L1 and L2 bands. Compared to the isolated antenna case, the proximity of the other device components as the battery or the casing causes a shift of the resonances towards the lower frequencies.

The total efficiency of the antenna over the same frequency range is shown in Figure 5(b). The antenna efficiency

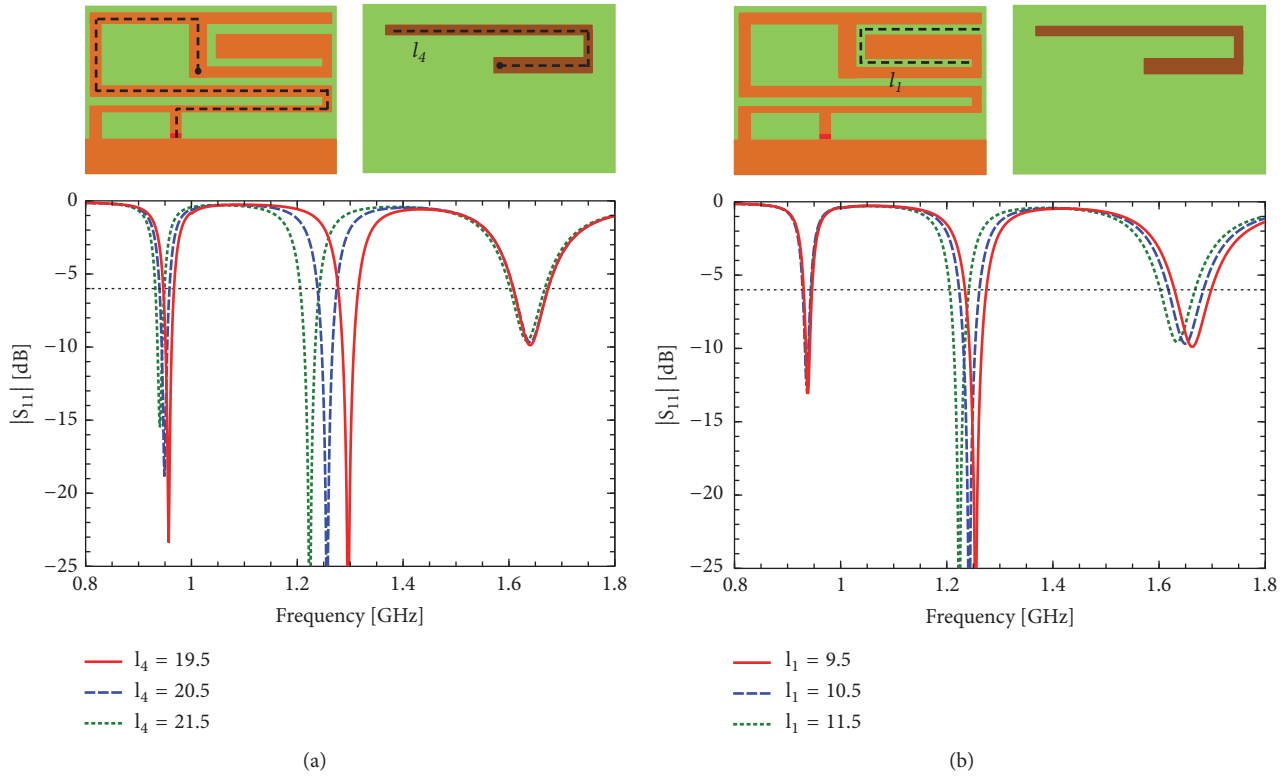

Figure 4: Variation of (a) the strip length l_4 and (b) the slot length l_1.

Table 1: Optimized antenna geometrical parameters [mm].

w	w_1	w_2	w_3	d_1	d_2	d_3	l_1	l_2	l_3	l_4
1.0	0.5	2.5	1.7	7.0	9.8	1.5	11.5	9.8	4.8	21.5

is about 30% over the LoRa band, 45% in the GPS L1 band, and 25% in the GPS L2 band. These values are acceptable for correctly receiving the GPS signal and transmitting the location information through the LoRa network, as it will be demonstrated in the final part of the paper, where field measurements of the tracking device are reported.

However, it is important to notice that such efficiency values can be mainly ascribed to the dimension of the antenna ground plane, which is limited by the compact size imposed on the IoT device ($0.12\lambda \times 0.08\lambda$ at 915 MHz). This is demonstrated in Figure 6, where the simulated antenna total efficiency for different lengths of the device is reported. The width of the device and the antenna geometry have been kept fixed. As can be observed, having a larger IoT device, which will have a bigger ground plane, would increase the antenna efficiency up to more than 65% in all the requested bands. However, this would make the overall IoT device much larger (up to 0.3λ), which does not meet the physical constraints imposed on the IoT device to be competitive on the IoT application market.

To further clarify this point, the performance of the proposed antenna has been compared to those of some state-of-the-art works dealing with antennas for small terminals. For each antenna presented in [11–13], Table 2 shows the antenna and terminal dimensions (expressed in λ at the lower operating frequency) and the corresponding declared efficiencies. The last line of Table 2 presents the same characteristics exhibited by the proposed antenna. As can be noticed, the total efficiency at the lower operating frequency (i.e., 915 MHz) of our antenna solution is lower than the ones presented in literature. However, our antenna is integrated into an IoT device that is much smaller (in length, 0.12λ vs. 0.24λ, 0.55λ, and 0.60λ). Consequently, in order to allow a fair comparison, starting from the results shown in Figure 6, the efficiency that the antenna would have if the device size was the same as the solutions presented in [11–13] is computed in the last column of Table 2. It becomes clear that, by integrating our antenna into a larger device (as the ones presented in literature), the efficiency of the proposed antenna will be larger than the state-of-the-art solutions.

3. Experimental Validation

In order to experimentally validate the numerical results, a prototype of the optimized antenna has been realized. As for the simulated model, two different prototype versions have been tested. The isolated version consists of only the antenna and the ground plane printed on the dielectric substrate,

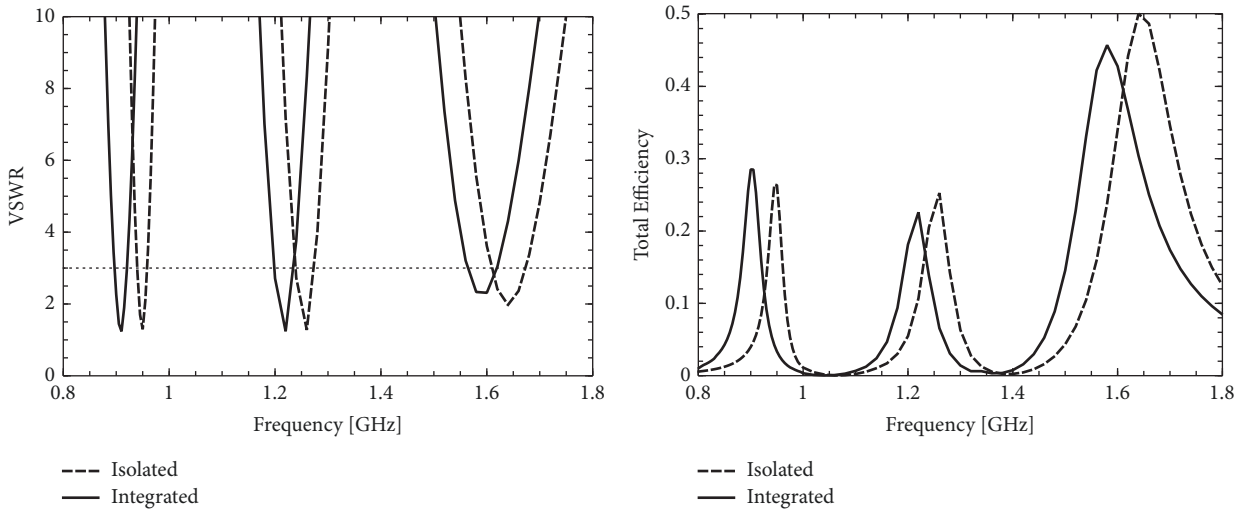

Figure 5: Simulated (a) VSWR and (b) total efficiency of the optimized antenna.

Table 2: Comparison of the proposed antenna with state-of-the-art solutions.

Solution	Antenna size (λ)	Terminal size (λ)	Total eff. (%)	**Proposed ant. equiv. tot. eff. (%)**
[11]	0.069×0.094	0.24×0.094	40	**55**
[12]	0.082×0.153	0.55×0.153	51	> **65**
[13]	0.085×0.34	0.60×0.34	56	> **65**
Proposed	$\mathbf{0.040 \times 0.076}$	$\mathbf{0.12 \times 0.076}$	**30**	

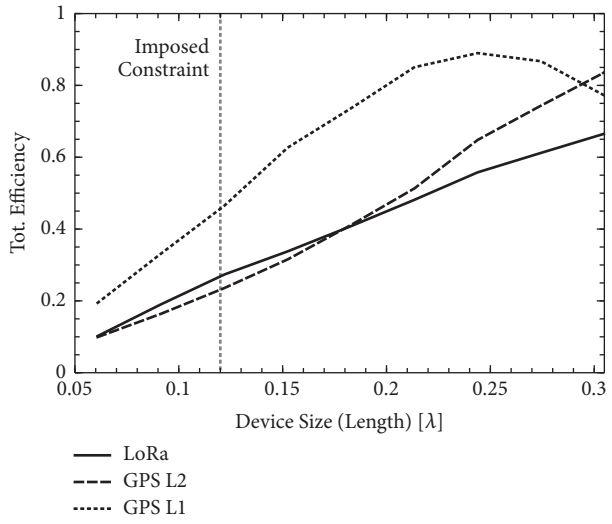

Figure 6: Antenna total efficiency in the 3 operating bands for different lengths of the IoT device.

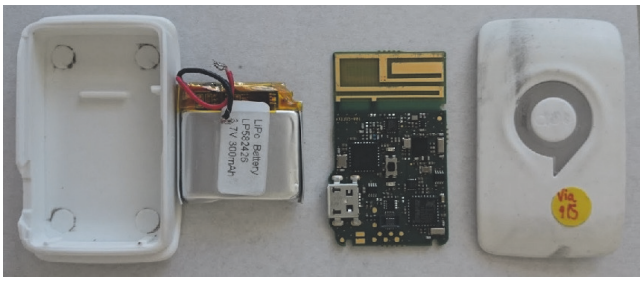

Figure 7: Antenna prototype printed on the PCB with the circuitry, the battery, and the casing.

while the integrated prototype includes the antenna, the PCB with all the electronic components, the battery, and the casing, all connected together (Figure 7).

As for the measurement protocol, all the data have been obtained in a MVG Starlab station operating in the frequency range 0.8-18 GHz. VSWR measurements have been obtained by directly connecting the antenna to a Rode & Schwartz ZVL13 vector network analyzer through a coaxial cable, while the radiating data (realized gain patterns and total efficiency) have been measured by putting the device transceiver (Semtech SX1272) into a constantly emitting mode without the need for a cable connection. This allowed the antenna to be tested in a realistic configuration avoiding for any unwanted cable effect.

Figure 8 shows the measured VSWR and total efficiency. As can be observed, the measured data confirm the capability of the integrated antenna to efficiently operate over the LoRa and the GPS bands. The measured data are in agreement with the numerical ones, validating the model of the antenna and

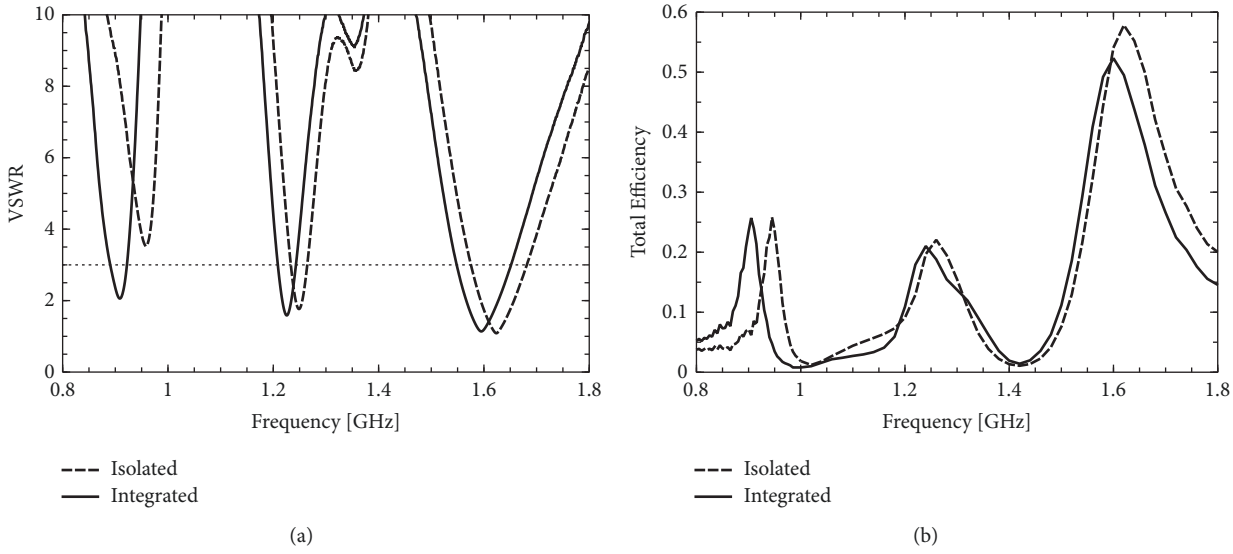

Figure 8: Measured (a) VSWR and (b) total efficiency of the optimized antenna.

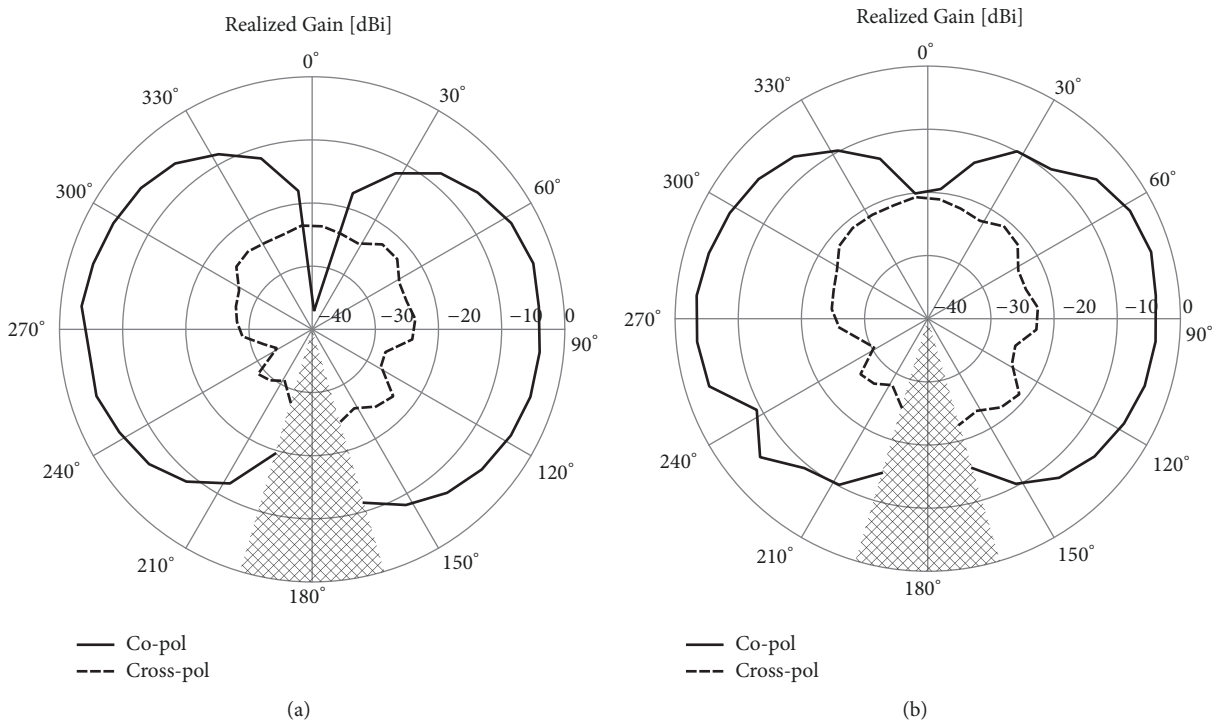

Figure 9: Measured realized gain patterns. (a) Plane at $\varphi = 0^\circ$ and (b) plane at $\varphi = 90^\circ$.

the IoT device used in simulations. Moreover, the measurements confirm the necessity of carefully keeping into account the environment close to the antenna during the design phase (e.g., the LoRa band is shifted from 960 MHz to 910 MHz). In the LoRa band, an operational bandwidth of 32 MHz centered on 910 MHz is obtained for a $VSWR \leq 3$ criteria. For the same matching criteria, a 103 MHz bandwidth centered on 1.578 GHz is measured for the GPS L1 band as well as a 35 MHz bandwidth centered on 1.22 GHz for GPS L2 band. Concerning the total efficiency, measured values are about 26% over the LoRa band, 52% in the GPS L1 band, and 20% in the GPS L2 band.

The measured radiation behavior of the prototype in the LoRa band at 915 MHz in the two vertical planes at $\varphi = 0^\circ$ and $\varphi = 90^\circ$ is shown in Figure 9. Gray sections indicate the location of the support for the antenna under test. As expected, the antenna exhibits the classical dipole-like radiation pattern typical of miniature antennas with a linear

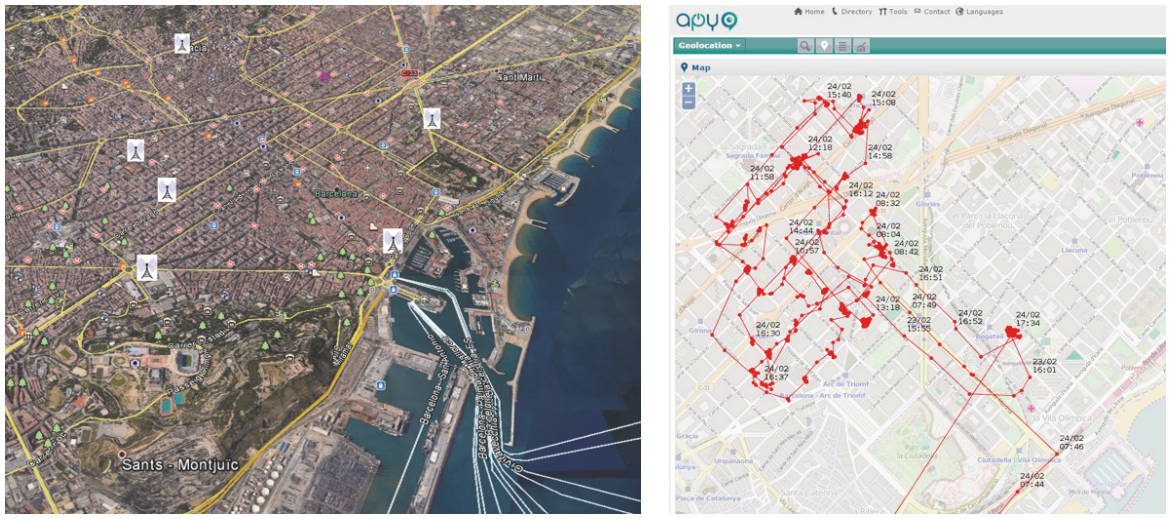

(a) (b)

FIGURE 10: IoT terminal field test. (a) LoRa base stations deployed in Barcelona, Spain, and (b) positions tracked by the device.

vertical polarization. The maximum realized gain at 915 MHz is about −3 dB. In the direction of maximum radiation, the cross-polar component is at least −15 dB lower than the copolar one, whatever the vertical plane.

4. Field Measurements

To evaluate the performance of the IoT position tracking device in a real scenario, in-field measurements have been performed in Barcelona, Spain, during the 2016 World Mobile Congress. Towards this end, some LoRa base stations have been deployed all around the city (Figure 10(a)). Successively, multiple copies of the realized device have been provided to a parcel delivery service. The IoT devices have been used to track the positions of the delivery trucks during the service. For example, Figure 10(b) shows the path done by one of the devices. According to the collected measurements, the maximum communication distance between the IoT terminal and the base station has been of about 12 km, when the average communication distance is about 3.5km, demonstrating the effectiveness of the designed LoRa radiating system in a real application. The average accuracy of the GPS positioning using only L1 band is about 5 meters.

5. Conclusion

In this paper, the design of an electrically small multiband antenna suitable for integration in a compact IoT terminal has been presented. An IFA structure has been properly modified to allow the antenna to cover multiple operating bands with good impedance matching and acceptable efficiency. The antenna has been optimized carefully taking into account the effects of the integration in the terminal. Measurements of the antenna as well as of the IoT device in a real scenario confirm the effectiveness of the proposed solution.

Data Availability

The simulated and measured data used to support the findings of this study are available from the corresponding author upon request.

Conflicts of Interest

The authors declare that they have no conflicts of interest.

Acknowledgments

The authors would like to acknowledge the CREMANT for its support in measurements.

References

[1] H. Wong, K.-M. Luk, C. H. Chan, Q. Xue, K. K. So, and H. W. Lai, "Small antennas in wireless communications," *Proceedings of the IEEE*, vol. 100, no. 7, pp. 2109–2121, 2012.

[2] J. Guo, L. Zhou, B. Sun, and Y. Zou, "Magneto-electric monopole antenna for terminal multiband applications," *IEEE Electronics Letters*, vol. 48, no. 20, pp. 1249-1250, 2012.

[3] M. A. C. Niamien, L. Dussopt, and C. Delaveaud, "A compact dual-band notch antenna for wireless multistandard terminals," *IEEE Antennas and Wireless Propagation Letters*, vol. 11, pp. 877–880, 2012.

[4] W.-W. Lee and Y.-S. Cho, "Frequency tunable antenna using coupling patterns for mobile terminals," *IEEE Electronics Letters*, vol. 51, no. 22, pp. 1725-1726, 2015.

[5] W. Liu, Z. Zhang, and Z. Feng, "ISM 433-MHz miniaturized antenna using the shielding box of mobile terminals," *IEEE Antennas and Wireless Propagation Letters*, vol. 11, pp. 330–333, 2012.

[6] J. Villanen, J. Ollikainen, O. Kivekäs, and P. Vainikainen, "Coupling element based mobile terminal antenna structures,"

IEEE Transactions on Antennas and Propagation, vol. 54, no. 7, pp. 2142–2153, 2006.

[7] M. R. Islam and M. Ali, "Ground current modification of mobile terminal antennas and its effects," *IEEE Antennas and Wireless Propagation Letters*, vol. 10, pp. 438–441, 2011.

[8] I. Szini, A. Tatomirescu, and G. . Pedersen, "On small terminal MIMO antennas, harmonizing characteristic modes with ground plane geometry," *Institute of Electrical and Electronics Engineers. Transactions on Antennas and Propagation*, vol. 63, no. 4, part 2, pp. 1487–1497, 2015.

[9] H. Liu, Y. Cheng, and M. Yan, "Electrically Small Loop Antenna Standing on Compact Ground in Wireless Sensor Package," *IEEE Antennas and Wireless Propagation Letters*, vol. 15, pp. 76–79, 2016.

[10] L. Lizzi, F. Ferrero, P. Monin, C. Danchesi, and S. Boudaud, "Design of miniature antennas for IoT applications," in *Proceedings of the 6th IEEE International Conference on Communications and Electronics, IEEE ICCE 2016*, pp. 234–237, vnm, July 2016.

[11] L. Zheng, X. L. Quan, H. J. Liu, and R. L. Li, "Broadband planar antenna based on CRLH structure for DVB-H and GSM-900 applications," *IEEE Electronics Letters*, vol. 48, no. 23, pp. 1443-1444, 2012.

[12] J.-H. Kim, Y.-B. Chae, J.-H. Lim, and T.-Y. Yun, "Printed internal antenna for mobile broadcasting (DVB-H/T-DMB) and communications (GSM900)," *IET Microwaves, Antennas & Propagation*, vol. 6, no. 6, pp. 680–684, 2012.

[13] Y. Wang and Z. Du, "A wideband quad-antenna system for mobile terminals," *IEEE Antennas and Wireless Propagation Letters*, vol. 13, pp. 1521–1524, 2014.